ISSN 0915-633X

NATIONAL INSTITUTE FOR FUSION SCIENCE

ELMy-H mode as Limit Cycle and Transient Responses of H-modes in Tokamaks

S.-I. Itoh, K. Itoh and A. Fukuyama

(Received – Mar. 22, 1993)

NIFS-221 May 1993

RESEARCH REPORT
NIFS Series

NAGOYA, JAPAN

ELMy-H mode as Limit Cycle and Transient Responses of H-modes in Tokamaks

Sanae-I. Itoh,
Research Institute for Applied Mechanics, Kyushu University
Kasuga, 816

Kimitaka Itoh,
National Institute for Fusion Science, Nagoya 464-01

Atsushi Fukuyama,
School of Engineering, Okayama University, Okayama 700
Japan

keywords: H-mode theory, Electric field bifurcation, ELMs, Giant ELMs, ELMy-H-mode, Limit cycle, Transient responses, Profile development

abstract

A model of Edge Localized Modes (ELMs) in tokamaks is presented. The model of the L/H transition, which is based on the electric field bifurcation, is extended to include the temporal evolution and the spatial structure. The existence of the electric field bifurcation infers a hysteresis curve between the plasma gradient(thermodynamic force) and the loss flux(flow). The time-dependent Ginzburg-Landau equation is formulated for the

electric field development, in which a limit cycle solution due to this hysteresis is contained. The self-generated oscillation of edge density appears, associated with periodic bursts of the loss, under the condition of constant particle flux from the core. This is attributed to the small and frequent ELMy activity in H-mode. Periodic decay and re-establishment of the transport barrier occur. This oscillation appears near the L/H transition boundary in the parameter space.

It is found that in H- and ELMy-H- states, the edge region forms an intermediate radial structure of diffusion coefficient (mesophase) between H-phase and L-phase. This is attributed to the transport barrier. Its radial structure is dictated by the ion shear viscosity. The diffusion Prandtl number, the ratio of the viscosity to the diffusivity, is found to determine the thickness of the barrier.

Phase diagram of L-, ELMy-H, H- and L/H bistable-states is obtained on plasma parameter space. To consider other types of ELMs, transient responses to the perturbations of the flux from the core are studied in each phase. In low collisionality plasma a sudden decrease of the flux can cause the transient bursting of a few ELMs before the L to H transition is completed. Large scale pulse from the core causes the transient return to L-phase and a giant burst occurs in high collisionality plasma. In ELMy-H state, external oscillations cause the mode-locking and other complicated dynamics (such as period doubling, trebling, and intermittent bursts). The perturbation in the flux widens the parameter regime of the occurrence of burstings.

§1 Introduction

Edge Localized Modes (ELMs) are regularly observed phenomena, characterized by the sudden drop of the edge density or temperature with a burst of plasma loss, during the H-phase in tokamak plasmas[1,2]. The ELMs have shown a variety in the magnitude and frequency of the bursts. The experimental characterization has begun and is under way[1,3-11]. Nevertheless, the key physical mechanisms discriminating the various ELMs remain unidentified.

A ELM with small and frequent periodic bursts has recently attracted attentions. This is because, at present, the improved confinement compatible with the efficient ash exhaust is only found in this operation mode. The parameter regime, where this kind of ELMs appears, has been found near the L/H transition boundary.[8,12,13] The physics understanding and the searching for the method to control ELMs are the urgent task.

The critical-β analysis due to MHD ballooning mode[3] has been applied to explain the ELMs. The analyses have shown that a class of ELMs occurs below the critical-β condition. Resistive MHD analysis[3] on a surface peeling mode may explain some of ELMs. However, the assumed current-pressure profiles are not yet experimentally identified. There remains a question whether all of ELMs can be explained by MHD instability models. For instance, the soft X-ray emission profiles of ELM activities do not shift when the surface q value is varied from 2.4 to 5.6,[3] which indicates that the ELMs are not necessarily localized at a cer-

tain rational surface. Furthermore, the period and the duration of small and frequent ELMs as well as the condition for the appearance remain unexplained.

To model the ELMs, a different approach has been made by introducing the impurity accumulation[14]. The impurity accumulation changes the electric field, and a cyclic oscillation between L and H phases takes place. However, the impurity accumulation can be considered as the independent phenomena[3,7] and should be treated separately.

Based on the bifurcation theory on the L/H transition[15-18], we have proposed a new and more complete model theory[19,20] of small and frequent ELMs observed in JFT-2M. The L/H transition has been observed to have a hysteresis curve on the phase plane of the thermodynamic force (such as density/temperature gradients) and of the associated flows of particle and heat.[1,3] The previous theories[15-18] are based on the static and 0-dimensional model of the transition through the bifurcations of the radial electric field and/or the poloidal rotation velocity. The bifurcation is dictated by the net radial current free condition. The current can be induced by the ion losscone loss[15-18], by the anomalous electron loss[15], by the ion viscosity[17] by the electron ripple loss[21] as well as by the external biasing. Experimental observations have been done[22-27], and have confirmed that there occur the changes in poloidal rotation and in radial electric field, associated with the L/H transition. DIII-D has shown that E_r jumps to a more negative value[22] (r being the minor radius). JFT-2M has confirmed the E_r change and re-

vealed that dE_r/dr becomes more negative[23]. Active biasing experiments on CCT[25] and TEXTOR[26] have shown that the L-H transition can be induced by both the positive and negative biasing. The rapid change in ion orbital loss of high energy part has recently been observed during the L/H transition on JFT-2M.[27] From these researches, it is understood that the L-H transition involves sudden change dE_r/dr and that, regardless of the sign of E_r, a picture of the bifurcation between multiple states is supported. The new model of the ELMs, which has been extended from the bifurcation models so as to include the temporal and spatial evolutions, has successfully shown that the bursts of the loss flux occur periodically owing to the hysteresis in the transport coefficient[19,20].

In this article, the self-sustaining oscillation is further studied. Based on the fact that the ELM's activity analyzed in Refs.[19] and [20] corresponds to a class of dynamic response of the H-mode, we analyze the temporal evolution of the L-mode and H-mode and examine the differences in the responses. Basic equations consist of the temporal evolutions of the electric field and the density, where the one-dimensional (i.e., radial) variation in space is kept. The region for appearing the self-generated oscillations is identified in the parameter space. The parameter dependence of the characteristic frequency is studied. The radial structure of the transport barrier in the H-phase is investigated and is compared with the L-phase. The important role of the ion shear viscosity to dictate the spatial structure is emphasized. We find that the diffusion Prandtl number, the

ratio of the viscosity and the diffusion coefficient, determines the barrier width. If this number is large, a thick transport barrier is formed, which would enhance the global confinement times. Some behaviors of the bursts and the parameter regime of their appearance are consistent with the observations on the small and frequent ELMs(near the L-H boundary)[11-13,19].

The dynamic response of the edge region to the external density modulation is analyzed. Three types of the perturbations in the flux from the core are considered; 1) a step-like change, 2) a pulsative change and 3) a sinusoidal oscillation. A step-like change can predict a few ELM's bursts before the final L/H(H/L) transition. Density pulse from the core causes the transient return path from the H-phase to the L-phase in the edge region. This process can predict both types of the bursts; that of the self-generated oscillations for a finite period and that of a large scale. When the modulation contains an oscillatory component, the mode with bursts which is locked to the external frequency (or to its harmonics) appears. If the modulation contains a random noise, the self-generated oscillation can be chaotic.

The construction of this article is as follows. In § 2, the model of the analysis is presented. The extension from the previous static analyses is shown. In §3, the one-dimensional transport equation is solved. Temporal and spatial evolution of the transport barrier is studied. In §4, the dynamic responses to external modulations are studied. Summary and discussion is given in the final section.

§2 The Model

The thin layer near the plasma edge, inside the outermost magnetic surface, of tokamaks is considered. The characteristic thickness of this layer is several times of the ion poloidal gyroradius, ρ_p. In this region the bipolar particle fluxes play an important role in determining the transport coefficient through affecting the radial electric field[15-18].

The static and 0-dimensional(0-D) model of the H/L transition[15-18] predicts the bifurcations of the radial electric field (or equivalently, the poloidal rotation). The net radial current free condition, $J_r=0$, determines the electric field. The current consists of electron and ion currents and the external one as

$$J_r(\text{boundary}) = \Sigma J_{\text{orbit}}^{(e,i)} + J_{\text{conv}} + J_{\text{bv}} + J_{\text{cx}} + J_{\text{ripple}}^{e} + J_{\text{ext}}$$

where $J_{\text{orbit}}^{(e,i)}$, J_{conv}, J_{bv}, J_{cx} and J_{ext}, which have the E_r and E_r' dependences, correspond to the currents driven by the electron or ion orbit loss(denoted by superscript, e and i), convective loss due to microscopic fluctuations, the bulk ion viscosity, the charge exchange loss, the ripple loss of electrons, and the externally injected current, respectively. Processes which are prominent near the plasma boundary are to be taken into account. When we identify and choose the dominant contributions to the

radial current, we find the solutions of E_r. Some solutions have multiple state, and the bifurcations of E_r and E_r' are predicted. Depending on the conditions imposed, the positive[15, 16, 21] as well as the negative[17, 18] jumps are predicted. The particle flux Γ and the transport coefficient D, which is defined by $-\Gamma n/\nabla n$ (where n is the density and ∇ is the gradient operator), are calculated as a function of the gradient near the plasma boundary. As the consequence of the nonlinear relation between the particle flux Γ and the density gradient, an S-figure curve is obtained as in Fig.1. Shown is the case for $J_r=J_{orbit}^{(i)} + J_{conv}$ and $E_r'=0$[16]. Even if $E_r'\neq 0$, a similar phase curve as in Fig.1 is obtained[18]. In both cases, the discontinuity of the flux occurs when the gradient parameter, $\lambda = \rho_p|\nabla n/n|$, reaches critical values λ_1 and λ_2. The critical values depend on the relative electron loss rate to the losscone loss rate, $d = \sqrt{a/R}D_e/\nu_i\rho_p^2$, where a/R is the inverse aspect ratio, D_e is anomalous electron diffusion coefficient in the L-phase, and ν_i is the ion collision frequency. In both cases of Refs.[14] and [16] the transition condition is roughly estimated as $d\lambda\sim 1$.

In the following, we consider the plasma of one ion species. The temperature is assumed to be uniform and constant. The effect of the temperature modulation is eliminated. Compared to the radial variation, the poloidal and toroidal variations are assumed to be small.

§2.1 Dynamical Equations

In extending the static model to the dynamical transport model, the transport equations for the electric field and for the plasma density are considered.

The equation dictating the temporal evolution of the radial electric field is given from the momentum equation of the poloidal direction, which is consistent with the Poisson's equation as,

$$\varepsilon_\perp \varepsilon_0 \, dE_r/dt = - J_r \qquad (1)$$

where $\varepsilon_\perp$ is the perpendicular dielectric constant of the magnetized plasma, in which the ion polarization current is included ($\varepsilon_\perp = 1+c^2/v_A^2$; v_A is the Alfven velocity and c is the speed of light). To study the radial profile of E_r, the viscous current, J_v, driven by the shear viscosity, μ_i, is included in J_r as, $J_r = J_r(\text{boundary}) + J_v$, where

$$J_v = \nabla \, [e\rho_p n_i / v_{Ti}] \mu_i \nabla (E_r/B_p), \qquad (2)$$

and we obtain,

$$\varepsilon_\perp \varepsilon_0 \, \partial E_r(r,t)/\partial t = e n_i \rho_p [-\nu_i \sqrt{R/a} \, J_b + \mu_i \nabla^2 (E_r/B_p v_{Ti})], \qquad (3)$$

J_b is the normalized quantity of the radial current at the boundary, $J_r(\text{boundary})$, v_{Ti} is the ion thermal velocity, B_p is the poloidal magnetic field. As has been shown in Refs.[15-21], the nonlinear dependence of J_r on E_r and E_r' gives rise to the bifur-

cations of $\Gamma(\lambda)$. For instance, $J^{(i)}_{orbit}$ is approximately given as

$$J^{(i)}_{orbit} = [C_F n_i \nu_i \rho_p / \sqrt{a/R}] \exp\{-Z^2\}. \quad (4)$$

where Z is the normalized radial electric field, and the coefficient C_F is a constant of the order of unity.

$$Z = C\, E_r \rho_p / T_i - Z_0 \quad (5)$$

where constants C and Z_0 are introduced as adjusting parameters. The dominant mechanism of electron loss determines the type of spontaneous transition. Depending on the loss mechanisms, either $L \rightarrow H^-$(the change of E_r associated with the transition, ΔE_r, is negative, $\Delta E_r < 0$)[17,18] or $L \rightarrow H^+(\Delta E_r > 0)$[15,21] is possible. In either case, the important physics ingredient is the hysteresis curve in the phase diagram of Γ-λ. And in both cases, the curve similar to Fig.1 is obtained. To obtain the analytic insight to extract the key physics, we choose an approximate curve as the model form for J_r. A model S-figure curve of the cubic equation, with

$$J_r(\text{boundary}) = J_1\, J_b(Z;g), \quad (6)$$

where, $J_1 = eC_F n_i \nu_i \rho_p / \sqrt{a/R} \simeq n\nu_* (T/rB)$ and

$$J_b = N(Z;g) = g - g_0 + [\beta Z^3 - \alpha Z] \quad (7)$$

$$g = d\lambda, \tag{8}$$

is employed. The normalized collision frequency ν_* is the ratio of ν_i to the bounce frequency of ions. Parameters α,β,g_0 in Eq.(7) are introduced for the approximation of the curve to simulate the physics process of concern. Parameters α and β dictate the sharpness at the ridge points λ_1 and λ_2 in Fig.1, and also their sign determines the type ($H^{\pm}$) of the transition. The parameter g is given as

$$g = \rho_p n'/n\nu_*, \tag{8'}$$

and g_0 denotes the point of inflection in the curve of $\Gamma(|\nabla n/n|)$. In the normalized form, Eq.(3) reduces to

$$\varepsilon \frac{\partial Z}{\partial t} = -(D_e/d\rho_p{}^2) J_b(Z;g) + \mu_i \frac{\partial^2 Z}{\partial x^2} \tag{9}$$

where the coefficient ε is approximated as

$$\varepsilon = (1+v_A{}^2/c^2)B_p{}^2/B^2 \simeq B_p{}^2/B^2.$$

and we take ε to be a smallness parameter.

When the plasma parameters and density profile are given, the value of g is determined. Solutions Z[g] are obtained through the net current free condition, $J_b(Z;g) = 0$, in the 0-D static models[15-18,21]. The curve of effective diffusivity D(Z[g]) as a

function of g is schematically shown in Fig.2. The hysteresis curve is projected on D-g plane and transitions occur at certain values of g, i.e. g_m and g_M. In the radial extent of x, where $g_m<g(x)<g_M$, the bifurcation is possible.

The density development is described by the continuity equation,

$$\frac{\partial n}{\partial t} = \frac{\partial}{\partial x} D(Z[g]) \frac{\partial n}{\partial x} \qquad (10)$$

where the particle source is neglected in the region considered here, and the flux is given as the boundary condition.

§2.2 Boundary Conditions

The slab region near the plasma edge is of our interest, $-L<x<0$. At the edge (x=0), we impose the constraint, that is,

$$(n'/n)^1 n^0 = \text{const.} \quad (\text{at } x=0) \qquad (11)$$

The condition (11) is chosen based on the two-dimensional transport analysis on the scrape-off layer (SoL) plasma[28]. The edge gradient was found to be less affected than the density itself even if the flux into SoL is varied. The particle flux from the core plasma (at x=-L) is treated as a parameter as

$$\Gamma = \Gamma_{in}. \qquad (\text{at } x=-L) \qquad (12)$$

§3 Solution of Self-generated Oscillation

§3.1 Numerical Model Equations

A set of equations are described in dimensionless forms as

$$\frac{\partial n}{\partial t} = \frac{\partial}{\partial x} D(Z) \frac{\partial n}{\partial x} \quad , \tag{13}$$

$$\varepsilon \frac{\partial Z}{\partial t} = -N(Z;g) + \mu \frac{\partial^2 Z}{\partial x^2} \quad , \tag{14}$$

where the modelled D(z) and the nonlinear term N are given as

$$D(Z) = (D_{max}+D_{min})/2 + (D_{max}-D_{min})/2 \cdot \tanh Z, \tag{15}$$

$$N(Z,g) = g-g_0+[\beta Z^3-\alpha Z]. \tag{16}$$

In the parameter regime of our interest, $\tanh Z \simeq Z$ holds. In order to study the distinction between L and H, we only keep the Z dependence in D, therefore, the radial profiles of D_{max} and D_{min} are taken to be uniform and constant. Normalization are employed as,

$$x/\rho_p \to x,\ D/D_0 \to D,\ d\mu_i/D_0 \to \mu,\ tD_0/\rho_p{}^2 \to t, \text{ and } \Gamma\rho_p/D_0 n_0 \to \Gamma.$$

n_0 is chosen to satisfy $g_0=1$ and $g = 3n^{-2}(dn/dx)$. D_0 takes a typical value of the L-phase. The coefficient μ is the diffusion

Prandtl number P_D [29]. Parameters g_0, α, β and μ are assumed to be constant.

Equation (14) is a kind of time dependent Ginzburg-Landau equation,[30] the one which is used to analyse the reaction diffusion system in chemical reactions.

§3.2 Periodic Formation of the Transport Barrier

Solving Eqs.(13)-(16) with the boundary conditions Eqs.(11) and (12), we find the solution with the periodic oscillations of the edge density, $n_s=n(x=0)$, and the loss flux, Γ_{out}, though Γ_{in} is constant in time. (Γ_{out} is defined as the particle flux at $x=0$.) The self-generating oscillation is found in the restricted region in the parameter space, i.e., near the transition layer of the L and H phases. In Fig.3 (a), (b) and (c), we show the temporal evolutions of the edge density(a), Γ_{out}(b) and their Lissajous figure(c). We take $g_0=1$, $\alpha=0.2$, $\beta=0.2$, $D_{max}=3$, $D_{min}=0.01$, $\mu=1$, $\varepsilon=0.01$, $r_n = -n/n'$ (at $x=0$) is chosen to be 1.25, and the constant flux at $x=-L$, $\Gamma_{in} = 3$.

In Fig.3 (d) and (e), the temporal change of the radial structures of the density and the effective diffusivity are shown. The diffusivity of L-phase is almost uniform, being close to D_{max} in this analysis and is shown by the dashed line. The structure of D in H-phase shows that the typical value of H-phase(lower branch in Fig.2) is only realized at the edge, and that the existence of intermediate state of L and H phases, i.e., the transport barrier with a finite extent, is seen in the radial structure of D. We call this mesophase. Associated with the

temporal change of D from H-phase to L-phase(Fig 3(e)), the burst of the flux, Γ_{out}, occurs. The state found here immanences the spatial region of the mesophase of the diffusion coefficient between the L and H phases. The temporal-spatial developments of the density and diffusion coefficient are shown by the bird's eye view in Fig.3 (f) and (g).

§3.3 Phase Diagram of L, ELMy-H and H-modes

In the space of the global plasma parameter, the oscillating solutions are only found near the transition boundary between the L and H phases. We attribute them to the small and frequent ELMs of the ELMy-H mode. The time-averaged density and the outflux are the intermediate values between those in L-phase and H-phase. Figure 4 illustrates the frequency as a function of $r_n(\propto\lambda^{-1})$.

Four regions are identified on the parameter space, namely, the low flux state, the state with periodic bursts, the high flux state and the bistable state of low flux and high flux. We call them, in the following, H-state region, ELMy(or ELMy-H)-state region, L-state region and bistable-state region, respectively. The phase diagram on $(d-\lambda/\sqrt{\Gamma_{in}})$ plane, corresponding to the model of Refs.[15,16], is shown in Fig.5. The parameter region in which the ELMy-H state appear is generally found to be

$$D_m/g_m < \Gamma_{in} r_n^2 < D_M/g_M, \qquad (17)$$

where

$$g_m = g_0 - 2\beta(\alpha/3\beta)^{3/2}, \tag{18-1}$$

$$g_M = g_0 + 2\beta(\alpha/3\beta)^{3/2}, \tag{18-2}$$

$$D_m = D(Z=\sqrt{\alpha/3\beta}), \tag{18-3}$$

and

$$D_M = D(Z=-\sqrt{\alpha/3\beta}). \tag{18-4}$$

When Γ_{in} becomes large and/or the edge density gradient(r_n^{-1}) is small so as to satisfy

$$\Gamma_{in} r_n^2 > D_M/g_M, \tag{19}$$

we find the stationary L-state. On the other hand, the H-state is found in the parameter region

$$\Gamma_{in} r_n^2 < D_m/g_m. \tag{20}$$

If the condition

$$D_m/g_m > D_M/g_M \tag{21}$$

holds, there appears the bistable state. Bistable region is shown by the hatched region in Fig.5. In such a case, direct and hard transition form L to H phase (or vice versa) occurs.

§3.4 Structure of Transport Barrier

Transport barrier with a finite radial extent is formed and is sustained in the H-phase. In the ELMy-H phase the periodic formation/destruction of the barrier takes place. It is known that the viscosity μ makes the radial structure of D be smooth [29,31]. Both in H and ELMy-H phases, the thickness of the barrier, Δ, is estimated in small μ limit as

$$\Delta \simeq \sqrt{2\beta\mu/\alpha}. \tag{22}$$

Numerical calculation gives $\Delta \propto \mu^{0.44}$ and confirms this estimate. (see Fig.6).

Note that the barrier width Δ is different from the width of the density profile change(density pedestal). As is shown in Fig.3(d,e), the variation in the density profile propagates deeper than the barrier width of D. The thickness of the transport barrier is determined by the viscosity, and the system size L does not affect either the frequency of self-generated oscillation or Δ.

§3.5 Period of Oscillations

The frequency of the self-generated oscillation in ELMy-H region τ^{-1}, is studied. Results for the model of Refs.[15,16] are shown by contour lines (dotted lines with numbers) in Fig.5. (The period τ is normalized to $\rho_p{}^2/D_0$.)

The numerical computation gives

$$\tau \simeq C\alpha r_n \Delta D_M^{-1}, \tag{23}$$

where C is a numerical coefficient of the order of unity ($C \simeq 3.5$). The dependence on Δ is also confirmed.(Fig.6(b)) For the existence of oscillating solution, the value of $\Gamma_{in} r_n^2$ is bounded as is given by Eq.(17). If D_M($\simeq$d in Fig.5) is varied, keeping the ratio r_n^2/D_M and other parameters fixed, we have

$$\tau^{-1} \propto D_M^{0.5}. \tag{24-1}$$

On the other hand, if Γ_{in} is varied, keeping the ratio $\Gamma_{in} r_n^2$ and other parameters fixed, we have

$$\tau^{-1} \propto \Gamma_{in}^{0.5}. \tag{24-2}$$

The ratio of the time interval of good confinement τ_H to the period τ, $\eta = \tau_H/\tau$, represents how this oscillating state is close to the H-mode. (In the H-mode, $\eta=1$ holds; $\eta=0$ for the L-mode). Figure 4 also illustrates η as a function of r_n. η takes an intermediate value between one and zero, being a decreasing function of $\Gamma_{in} r_n^2$, and is discontinuous at the boundaries D_m/g_m and D_M/g_M. For oscillating solutions, η takes the largest value η_{max} at $\Gamma_{in} r_n^2 = D_m/g_m$, and η_{max} approaches to unity if D_m becomes close to D_{min}. This tells us a possibility to control the ratio of the pulse width and the period.

§3.6 Correspondence to A Transition Model

The relation between coefficients (α, β, D_{max}, D_{min}) and the plasma parameters is considered with respect to the model of Refs.[15,16]. In this model, relations

$$d\lambda \sim 1 \qquad (\text{at } \lambda=\lambda_1[d]) \tag{25-1}$$

and

$$d\lambda \sim 2\lambda^2\exp(-\lambda^2) \qquad (\text{at } \lambda = \lambda_2[d]) \tag{25-2}$$

hold as a rough estimate. At the transition points, λ_1 and λ_2, we have the approximate relations

$$g_M = \frac{2}{1+dQ} \qquad g_m = \frac{2dQ}{1+dQ} \tag{26-1}$$

and

$$D_M = d\{1-\frac{d^2}{2}\} \qquad d_m = \frac{d}{2Q^2} \tag{26-2}$$

where

$$Q = \sqrt{\ell n(\frac{2e}{d}) + \frac{1}{2}\ell n\left|\ell n(\frac{2e}{d})\right|}\ . \tag{26-3}$$

In the parameter regime of our interest where $\tanh Z \simeq Z$ holds, α and β is implicitly expressed by d as $\alpha = 3h(1-dQ)/\{2(1+dQ)\}$, and $h = \sqrt{3\beta/\alpha}$. In this case, D_{max} and D_{min} are expressed as

$$D_{max} = d(1-d^2/2)(1+h) + (1-h)Q^{-2}/2 \qquad (27\text{-}1)$$

$$D_{min} = d(1-d^2/2)(1-h) + (1+h)Q^{-2}/2. \qquad (27\text{-}2)$$

If other bipolar loss is dominant to cause J_r, parameters (α, β, D_{max}, and D_{min}) may have other dependences on plasma parameters.

§4 Transient Responses and An Application to Giant ELM

Variety of dynamic responses to external perturbation are found in each phase from model equations. In this section, we examine the responses associated with the modulations of the particle flux Γ_{in}. Three types of the perturbation are considered, i.e., 1) a step-like change, 2) short pulse, and 3) periodic oscillations in the flux, Γ_{in}. These dynamical perturbations, for example, open up the paths on a phase diagram of Fig.5. Cases are shown below.

§4.1 Step-like change

Suppose that the plasma edge is initially in the L-phase, (A point in Fig.7) and that the influx is suddenly reduced to the level of H-phase for the other fixed parameters. Then the edge plasma follows a trace A → A' and finally reaches to a stationary H-phase. In this case, the plasma passes the ELMy region along the line, a few self-generated ELMy pulses appear before the H-phase is established. The numerical calculation from our model is shown in Fig.8. The edge plasma is initially in the L-phase (at t=0, Γ_{in}=6) and the Γ_{in} is suddenly reduced to 1 at the coreside of the edge plasma(x=-4)(see Fig.8(a)). Then we observe a few periodic bursts in the outflux from the plasma surface(x=0) (Fig.8(b)). The time delay is due to the radial transport of the flux. Associated with this dynamical change of Γ_{in}, the edge takes place the transition to H-phase. The radial structures of the density and D are shown in Fig.8(c and d) respectively. This

case is seen when the plasma takes the path on the diagram(Fig.7), similar to A → A'. Inverse process(A' → A), namely, the H-phase → A few ELMy state → L-phase, is also possible.

If the initial influx corresponds to the H-phase and the final one is for the ELMy-H state, a path like B → B' is opened in Fig.7. In Fig.9, the case is shown where the flux Γ_{in} is step-likely increased at t=0 from Γ_{in}=1 to Γ_{in}=4. The bursts of higher frequency appear before the steady bursts continue to occur. Along the path B → B', the characteristic frequency of the oscillations becomes lower as is shown by the contour lines in Fig.7. This is observed in this calculation. Note that the state during a few ELMs is not either in the L-phase or in the H-phase. An inverse process is also possible.

§4.2 Pulsative change

When the positive pulse in particle flux is supplied from the core for a short period, a few ELM's bursts appear. The model calculation is shown in Fig.10. The density pulse with its hight Γ_{in}=4 and its period Δt=2 is applied to the H-state (Γ_{in}=1) at t=0. The path like B → B' → B is opened, and the plasma finally comes back to the original state, after bursting the pulse in the form of a few ELMs. This is shown in Fig.10. Depending on the fluence of the pulse, $\Delta n \equiv \Delta\Gamma_{in}\Delta t$, the response changes. If the pulse is too small for the edge plasma to cross the boundary between the phases on the diagram, the edge remains the same phase and just a small modification of the outflux appears. Similar arguments apply to the negative pulse of the particle

flux.

If the plasma takes a small value of $d \equiv \sqrt{a/R} D_e / \nu_i \rho_p^2$, the hard transition takes place in high λ bistable region.(Hatched region in Fig.5) The small value of d is realized when the plasma is collisional(high density) or ion loss channel dominated (i.e., electron loss, D_e, is small), and/or small B_T case etc. Near this regime, a different impulse response is seen. If the plasma is initially in the H-phase(C point in Fig.8), the large pulse of Γ_{in} causes a giant pulse of the outflux. The edge plasma experiences the one cycle of the hard transition curve as schematically shown in Fig.2.(B → B' → A' → A → B). The radial change of the effective D, namely $\Gamma = -D\nabla n$, and the density profile are plotted vs time in Fig.11. The resultant outflux is also shown as a function of time. Even if the plasma is deep in the H-phase, the large influx can cause this kind of giant pulse associated with the density increase near the edge. In this case Γ_{in} increases and d decreases. This is attributed to a Giant ELM activity. Therefore, some ELMs are possibly considered to be the responses to the changes of the flux.

§4.3 Periodic external oscillations

The regular temporal change of the flux is driven by saw-toothing from the core. When the plasma is rotating with the helical deformation, the periodic plasma/wall interaction causes the modulation of the particle flux even from the outside.

To simulate both of the external perturbations, we reduce the 1D model to 0-D model. The Γ_{in} is projected to a parameter

$S(\equiv \Gamma_{in}/\bar{\Delta}$, where we take $\bar{\Delta}$ to be the averaged value of Δ, being constant in 0-D model). We introduce a temporal change in S as

$$S = S_0 + \varepsilon_f \cdot \sin(2\pi\Omega t). \tag{28}$$

Coefficients S_0, ε_f and Ω are constant in time.

We study the effect of an external oscillation near the ELMy-H region ,e.g. along A-A' in Fig.7. The applied frequency is close to the self-generated one, $\Omega \sim 1$. Figure 12 summarizes the results on the phase diagram in S_0-ε_f plane. The change in S_0 corresponds to the change in Γ_{in}. As ε_f increases, the region of oscillating solution expands to the wider values in S_0.

The oscillation region is mainly divided into three. One is shown by the shaded region, where the original frequency is almost preserved. The second is the 'locked region' denoted by 1, where mode locking to the applied frequency takes place. In the periphery of the oscillation regime(the third), the period doubling takes place, i.e., the frequency of the generated oscillation is one half of the applied frequency (denoted by '1/2'). Trebling and higher harmonics generations also occur. Intermittent burst of loss, the interval of which approaches to $1/2\pi$, is observed. Some are already reported by use of 1-D model[20].

The aperiodic region, shown by L or H, also exists. The case where Ω is much lower/higher than the intrinsic frequency of self-generated oscillation is also studied. Similar arguments to the case of Fig.12 applies. Also a strong influence is seen near the phase boundary. If the modulation contains a random noise, the self-generated oscillation is found to be chaotic.

§5 Summary and Discussions

In summary, the electric field bifurcation model for the H/L transition is extended to include the temporal and spatial evolutions of the radial electric field and the plasma density. The time-dependent Ginzburg-Landan equation, which includes the spatial diffusion as well as the nonlinear terms, is formulated for the development of the electric field, Z. The radial electric field dictates the effective diffusion coefficient, D[Z(g)], which then affects the density profile. The temporal and spatial developments of the plasma density is simultaneously solved in our set equations. The solutions of the model equations tell us 1) how the plasma dynamics takes place between L-phase and H-phase and 2) how the profiles of the transport barrier and of the density develop near the plasma edge.

The stationary solution of high(low) flux corresponds to the L(H)-phase. In the H-phase, the transport barrier of the finite radial width is formed near the edge.(Fig.3(e,d)) Between H- and L-phases, there obtained a solution in which the self-generated oscillation of the outflux, Γ_{out}, and the edge density occur under the constant influx condition from the core.(Fig.3) This is accompanied by the successive decay and formation of the transport barrier. The magnitude of the time-averaged outflux is intermediate value between those in the L-phase and the H-phase. The value η is introduced to quantify the confinement improvement. We attribute this state to ELMy-H state and call this phase to be a mesophase(between L and H).

The phase diagram is obtained for the physics model of L/H transition in Refs.[15,16,18]. The d - $\lambda/\sqrt{\Gamma_{in}}$ plane is divided into four regions, namely L-state, ELMy-(ELMy-H)state, H-state and L-H bistable state.(Fig.5) The characteristic frequency in ELMy-H state is studied. The transport barrier width of the H-state(and the ELMy-H state) is found to be roughly proportional to $\sqrt{\mu}(\mu^{0.44}$:numerical). Its temporal evolution in ELMy-H state is also shown.

Transient responses to external perturbations in the flux are examined in each phase. The dynamical change of the particle flux makes the path on the phase diagram(Fig.7). Three types of the perturbation are examined, namely, a step-like change, a pulsative change and a sinusoidal oscillation. Variety in responses is shown from our simple model equations. It is demonstrated that, because of the step-like change in the influx, there exists a few ELM's burst before the L- to H-phase transition(Fig.8). As the response to a pulse, a few ELM's burst(Fig. 10) or a Giant ELM(Fig.11) is induced. A few ELM's burst occurs when the plasma passes through the intermediate-state(ELMy-state), and a Giant ELM is induced when the edge enters into a bistable-state. The appearance of the bursts is found to depend on 1) where in the phase diagram the initial state of the plasma is located, 2) what type of the perturbation is applied, 3) how large the external perturbation is, 4) what time scale the perturbation has, and so on.

The responses to the sinusoidal perturbation are found to have much variety. In particular, in ELMy-state there occur the

self-generated oscillation of the bursts with mode-locking, period doubling, trebling, higher harmonics generations, and intermittency to the applied external perturbation. The strength of the perturbation widens the ELMy-H state.(Fig.12)

Our model equations consist of the temporal and spatial evolutions of E_r(poloidal velocity) and n(r) near the edge. Coupling neither to the temperature evolution nor to the velocity in different direction is considered. Each coupling can, in principle, predict the similar results which are obtained in this article. The parameter space of the phase diagram alters and the parameter dependences may change. If an additional equation is added to our model equations, there appear a new physics process. These are left for future works.

The model equations are applied to a particular physics model of L/H transition, and the parameter dependences are shown. Depending on the physics model of J_r, the correspondences of the physics quantities to the parameters introduced in our model curve change. There have been reports on the other contributors to cause J_r, such as the electron ripple loss, impurities, the loss due to the high energy ion component and so on. Each should be examined separately and the combined effect should also been studied. Analysis in this article utilizes a simplified form, and concentrates to explore the basic physics picture. Further analysis may show the variety in various processes.

The self-generated oscillations, which are predicted to occur near the L/H transition boundary, are consistent with the experimental observations of the small and frequent ELM activity

[10-12,19]. If the electron loss becomes large, i.e., $D_e(d)$ is large, not a hard transition but a ELMy activity is predicted from our model. This might be the case, when Ergodic Magnetic Limiter[6,11] is applied, the hard transition diminishes and the small and frequent ELMs appear.

The Prandtl number is shown to dictate the barrier width, i.e., the region of sheared poloidal rotation. The width of the transport barrier needs further comparison study with experiments. The simultaneous measurements of the viscosity, diffusion coefficient and the width will answer the question. The Prandtl number also dictates the density profile of core plasma, i.e., the peakedness of density profile. [32,33] From the profile measurements of toroidal rotation, an agreement has been observed.[34]

The observation of the fine structure of a burst in time will explore the type of the transition. If it is originally a hard transition type, the sudden decrease of the loss is predicted to occur at the end part of each burst. The time scale would be the same as that of the sudden increase of the loss at the onset of the burst. Because of the long response time due to neutral recycling, the observation of $H\alpha/D\alpha$ line can not distinguish it. The discrimination would be possible by high time resolution measurement of the heat deposition onto the divertor plate during a whole burst.

The analysis of the effect of external oscillations on the ELM activities indicates a possible method to control ELMs. The self-generated oscillation can be locked to the external oscillation, which will then be controlled from outside.

Acknowledgements

Authors acknowledge discussions with Prof. T. Ohkawa, Dr. Y. Miura and JFT-2M Group, Dr. S. Konoshima and DIII-D group, Drs. K. Ida, S. Kaye and H. Zohm. Comments by Prof. A. Lichtenberg is also appreciated. This work is partly supported by the Grant-in-Aid for Scientific Research of MoE Japan, and by the collaboration program between universities and JAERI on fusion research.

References

[1] M. Keilhacker, G. Becker, K. Bernhardi, et al.: Plasma Phys. Controlled Fusion **26** (1984) 49.

[2] F. Wagner, G. Becker, K. Behringer, et al.: Phys. Rev. Lett. **49** (1982) 1408.

[3] The ASDEX Team: Nucl. Fusion **29** (1989) 1959.

[4] P. Gohil, M. A. Mardavi, L. Lao, et al.: Phys. Rev. Lett. **61** (1988) 1603; D. H. Hill, T. Petrie, M. A. Mardavi, et al.: Nucl. Fusion **28** (1988) 902; D. P. Schissel, K. H. Burrel, J. C. DeBoo, et al: Nucl. Fusion **29** (1989) 185.

[5] DIII-D Team: in Plasma Physics and Controlled Nuclear Fusion Research, 1990, Proc. 13th IAEA International Conference, Washington DC USA, (1990) Vol.1, p69.

[6] T. Shoji, and JFT-2M Group: in Controlled Fusion and Plasma Physics (Proc. 17th European Conf., Amsterdam, 1990), Part3, (1990) 1452.

[7] F. Wagner, F. Ryter, A. R. Field, et al.: in Plasma Physics and Controlled Nuclear Fusion Research, 1990, Proc. 13th IAEA International Conference, Washington DC USA, (1990) Vol.1, p277.

[8] Y. Miura and JFT-2M Group: in Plasma Physics and Controlled Nuclear Fusion Research, 1990, Proc. 13th IAEA International Conference, Washington DC USA, (1990) Vol.1, p325.

[9] T. Osborne, K. H. Burrell, T. Carlstrom, et al: Bull. Am. Phys. Soc. **35** (1990) 1975.

[10] Y. Miura and JFT-2M Group: private communications (invited

paper presented in the 3rd H-Mode Workshop (JET, 1991).

[11] Y. Miura, T. Shoji, M. Mori, et al.: Kakuyugo Kenkyu **66** (1991) 267 (in Japanese).
S. Konoshima, R. D. Stambaugh, H. Matsumoto, et al.: Kakuyugo Kenkyu **66** (1991) 413 (in Japanese).

[12] K. Shimizu: private communication(also JAERI memo 01-478, unpublished).

[13] Y. Kamada and M. Mori: private communication on JT-60U experiments, also papers presented at Japan-US workshop on "Transient phenomena in Toroidal Plasmas" (San Diego, Jan. 1993).

[14] T. Ohkawa, S.-I. Itoh, and K. Itoh: Kakuyugo Kenkyu, **59** (1988) 488.

[15] S.-I. Itoh, K. Itoh: Phys. Rev.Lett. **60** (1988) 2276.

[16] S.-I. Itoh and K. Itoh: Nucl. Fusion **29** (1989) 1031.

[17] K. C. Shaing, E. C. Crume: Phys. Rev. Lett. **63** (1989) 2369.

[18] S.-I. Itoh and K. Itoh: J. Phys. Soc. Jpn. **59** (1990) 3815.

[19] S.-I. Itoh, K. Itoh, A. Fukuyama, Y. Miura and JFT-2M Group: Phys. Rev. Lett. **67** (1991) 2485.

[20] S.-I. Itoh, K. Itoh and A. Fukuyama: in Plasma Physics and Controlled Nuclear Fusion Research, 1992, 14th IAEA International Conference, Wurzburg Germany(1992), paper IAEA-CN-56/D-4-19.

[21] K. Itoh and S.-I. Itoh: Nucl. Fusion **32** (1992) 2243.

[22] R. J. Groebner, K. H. Burrel, R. P. Seraydarian: Phys. Rev. Lett. **64** (1990) 3015.

[23] K. Ida, S. Hidekuma, Y. Miura, T. Fujita, M. Mori, K.

Hoshino, N. Suzuki, T. Yamauchi, JFT-2M Group: Phys. Rev. Lett. **65** (1990) 1364.

[24] C. E. Bush, N. L. Bretz, E. D. Fredrickson, et al: in Plasma Physics and Controlled Nuclear Fusion Research, 1990, Proc. 13th IAEA International Conference, Washington DC USA, (1990) Vol.1, p309.

[25] R. J. Taylor, M. L. Brown, B. D. Fried, H. Grote, J. R. Liberati, G. J. Morales, P. Pribyl, D. Darrow, M. Ono: Phys. Rev. Lett. **63** (1989) 2365.

[26] R. R. Waynants, D. Bora, T. Delvigne, et al.: in Plasma Physics and Controlled Nuclear Fusion Research, 1990, Proc. 13th International Conf., Washington DC USA, (1990) Vol.1, p473.

[27] Y. Miura, F. Okano, N. Suzuki, M. Mori, K. Hoshino, H. Maeda, T. Takizuka and JFT-2M Group, S.-I. Itoh and K. Itoh: Phys. Rev. Lett. **69** (1992) 2216.

[28] S.-I. Itoh, N. Ueda, and K. Itoh: Plasma Phys. Controlled Fusion **32** (1990) 415.

[29] E. M. Lifshiz and L. P. Pitaevskii: Fluid Mechanics, Landau and Lifshiz Course of Theoretical Physics **6** (Pergamon, Oxford, 1987), Cap. V1.

[30] E. M. Lifshiz and L. P. Pitaevskii: Statistical Physics Part 2, Landau and Lifshiz Course of Theoretical Physics **9** (Pergamon, Oxford, 1980) Sec.45.

[31] E. Yahagi, K. Itoh, M. Wakatani: Plasma Physics and Controlled Fusion **30** (1988) 995.

[32] S.-I. Itoh: J. Phys. Soc. Jpn. **59** (1990) 3431.

[33] K. Itoh, and S.-I. Itoh: Comments on Plasma Phys. Controlled Fusion **14** (1991) 1.

[34] K. Ida, S.-I. Itoh, K. Itoh, S. Hidekuma, Y. Miura, H. Kawashima, M. Mori, T. Matsuda, N. Suzuki, H. Tamai, T. Yamauchi and JFT-2M Group: Phys. Rev. Lett. **68** (1992) 182.

Figure Captions

Fig.1 Normalized particle flux Γ as a function of gradient parameter λ for various values of d. The momentum loss by neutral particles is not taken into account. (Quoted from Ref.[16] with corrections).

Fig.2 Model of effective diffusivity D (i.e., ratio of the particle flux to the density gradient) as a function of gradient parameter g. See text for the definition and normalization. (α=1, β=1, D_{max}=3, D_{min}=0.1, g_0=1).

Fig.3 Temporal evolution of edge density n_s (a) and outflux Γ_{out} (b). Parameters are μ=1, Γ_{in}=3, r_n=1.25, α= β= 0.2, D_{max}=3, and D_{min}=0.01. Trajectory in (n_s-Γ_{out}) space is given in (c). Spatial profiles of density (d) and diffusivity (e). The time sequence is indicated by A, B, C, D with arrows in (a) and (b). Solid and dashed lines in (d) and (e) show the profiles before the burst and at the end of the burst. The time slices, A, B, C and D are also marked in (e).

Fig.4 The characteristic frequency (solid line) and the 'H-ness' parameter η(dashed and dotted line) are shown as a function of $r_n(\lambda^{-1})$. Γ_{in}=3 and other parameters are standard as in Fig.3.

Fig.5 The regions of L-, ELMy H-, and H-modes are shown in the $d-\lambda(0)/\sqrt{\Gamma_{in}}$ plane. Bistable region of the H- and the L-mode is shown by the shaded area. Dotted contour lines in ELMy region indicate the frequency of self-generated oscillation normalized to $D_0/\rho_p{}^2$.

Fig.6 The μ-dependence of the thickness of the transport barrier Δ (a), and the oscillation period τ (b), are observed as $\Delta \propto \mu^{0.44}$ and $\tau \propto \mu^{0.44}$. $\alpha=\beta=0.2$, and other parameters are standard values as in Fig.3. The analytic estimate is confirmed.

Fig.7 Paths caused by the perturbation in the influx, Γ_{in}, are schematically drawn on the phase diagram of Fig.5. A step-like reduction of Γ_{in} opens the path A → A', which is associated with a transient ELMy-state (Fig.8); a step-like increase makes B → B' (Fig.9); a positive pulse causes B → B' → B (Fig.10). The pulsative increase of both Γ_{in} and D_0 opens the round path from C to C.(Fig.11)

Fig.8 A step-like reduction of Γ_{in} at the core side(x=-4) at t=1 (a) causes the H to L transition associated with a few ELM bursts(b). The changes of radial structures of the density(c) and D(d) are shown by dashed lines(initial L-phase) and by solid lines(final H-phase).

Fig.9 A step-like increase of Γ_{in} makes a path of B → B' in Fig.7, and causes the L → ELMy phase transition. At t=0, Γ_{in} is increased from 1 to 4. Other parameters are the same as those in Fig.3. The changes in n_s and Γ_{out} are shown.

Fig.10 A positive pulse causes a path like B → B' → B in Fig.7. As the response of the H-phase, only a few ELMs appear. At t=0, Γ_{in} is creased from 1 to 4, and at t=2, Γ_{in} is reduced to 1. Other parameters are the same as that in Fig.3.

Fig.11 A Giant ELM is caused as a response of the pulsative increase of D inside part of the transport barrier. The local enhancement of D is made in the region of $-2.0 < x < -1.0$, during the period of $5.0 < t < 6.0$, by the additional value of 3. The barrier width Δ is $\sqrt{2}$. Bird's eye view of the density profile development shows the local flattening inside the barrier(a). A giant pulsative outflux at the edge is shown as a function of time(b).

Fig.12 Phase diagram in the presence of the external oscillation in the source($S=\Gamma_{in}/\bar{\Delta}$) is plotted on the plane of constant component S_0 and oscillation amplitude ε_f. Frequency of the external oscillation is fixed to be $\Omega=1(\alpha=0.5, \beta=1)$. The line of $\varepsilon_f=0$(a horizontal axis)

is divided into L, ELMy and H regions, and according to the increase of ε_f, the ELMy region expands. Original oscillation prevails in the shaded region(a). Mode locking and the locking to subharmonics are found. Number j/k (such as 1, 1/2, 1/3, 2/3, 3/4 ...) indicates that the mode locking with j/k harmonics to the external frequency occurs in this region. Expanded diagram is given in (b). In shaded area in (b), a random oscillation takes place.

Fig.1

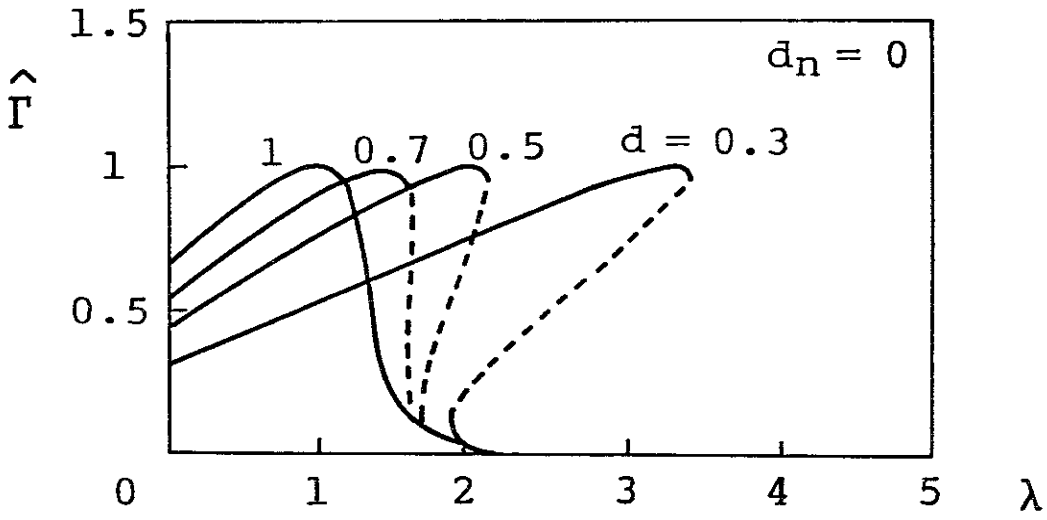

Fig.2

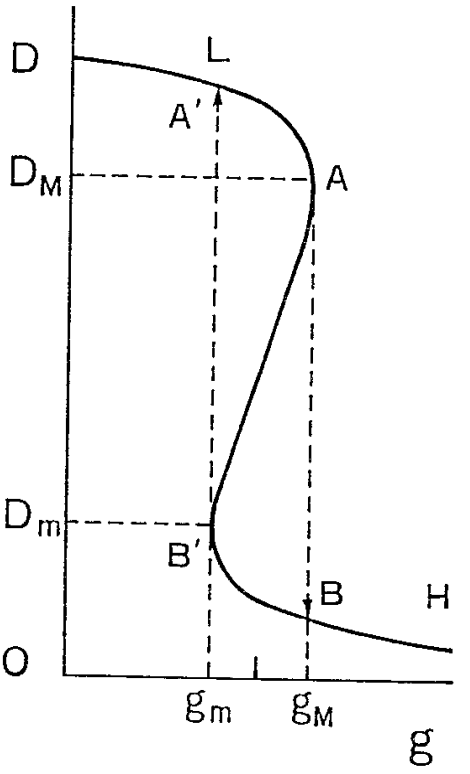

Fig.3

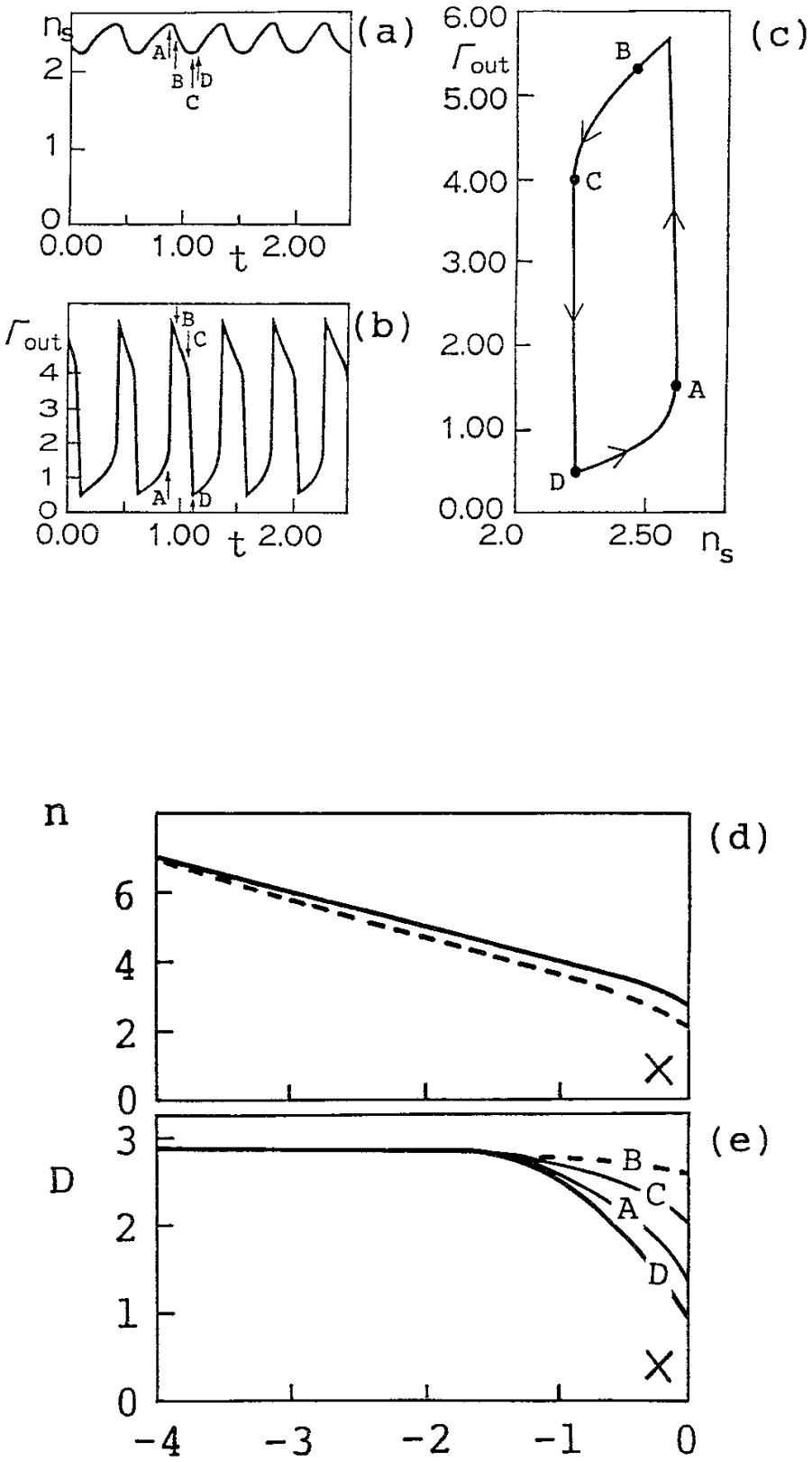
(a)
n_s
2
1
0
A
B
C
D
0.00
1.00
t
2.00
(b)
Γ_{out}
4
3
2
1
0
B
C
A
D
0.00
1.00
t
2.00
(c)
6.00
Γ_{out}
5.00
4.00
3.00
2.00
1.00
0.00
B
C
A
D
2.0
2.50
n_s
n
(d)
6
4
2
0
X
D
(e)
3
2
1
0
B
C
A
D
X
-4
-3
-2
-1
0

Fig.4

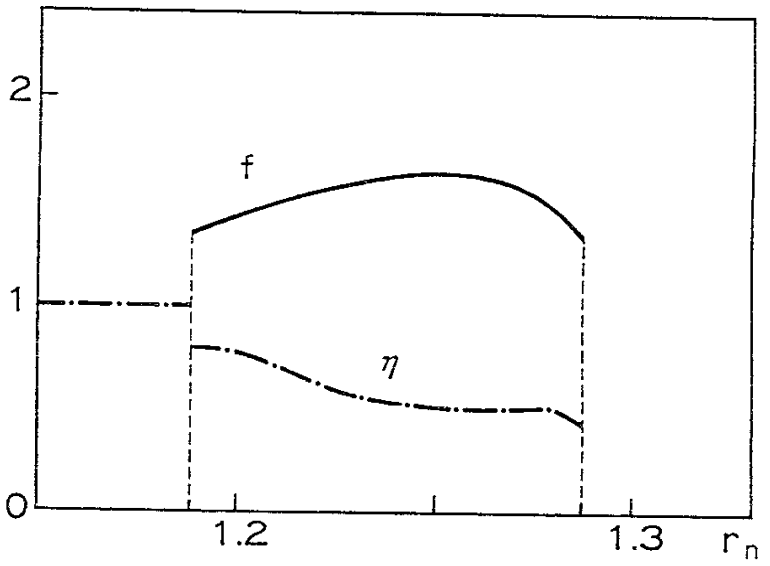

Fig.5

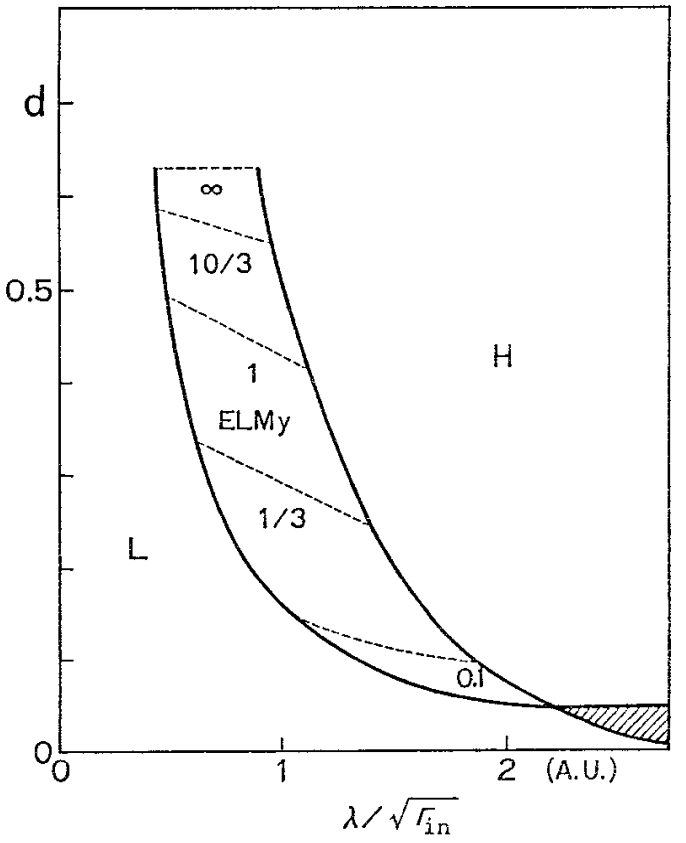

Fig.6

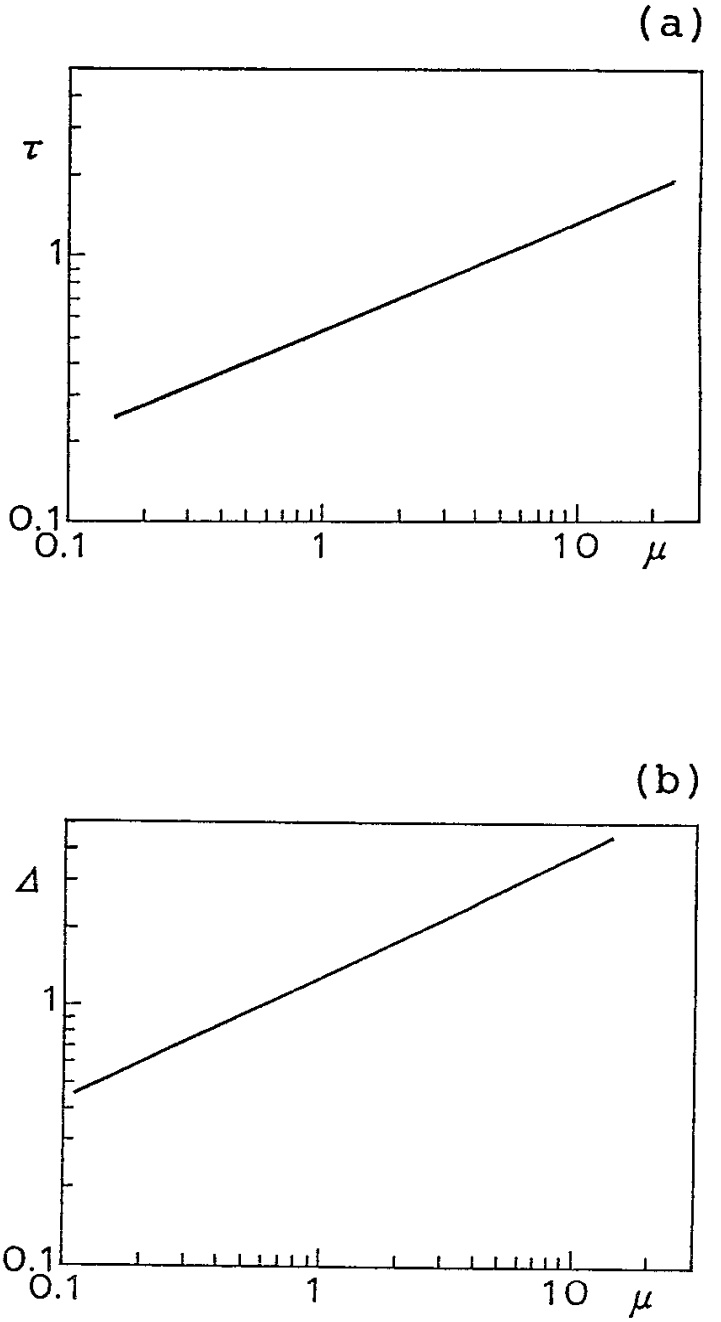

Fig.7

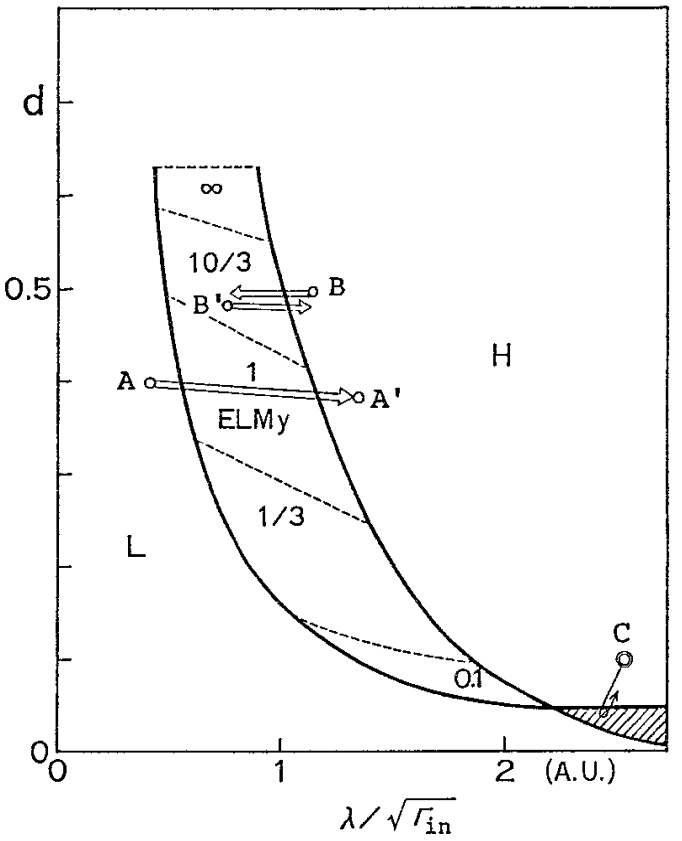

Fig.8

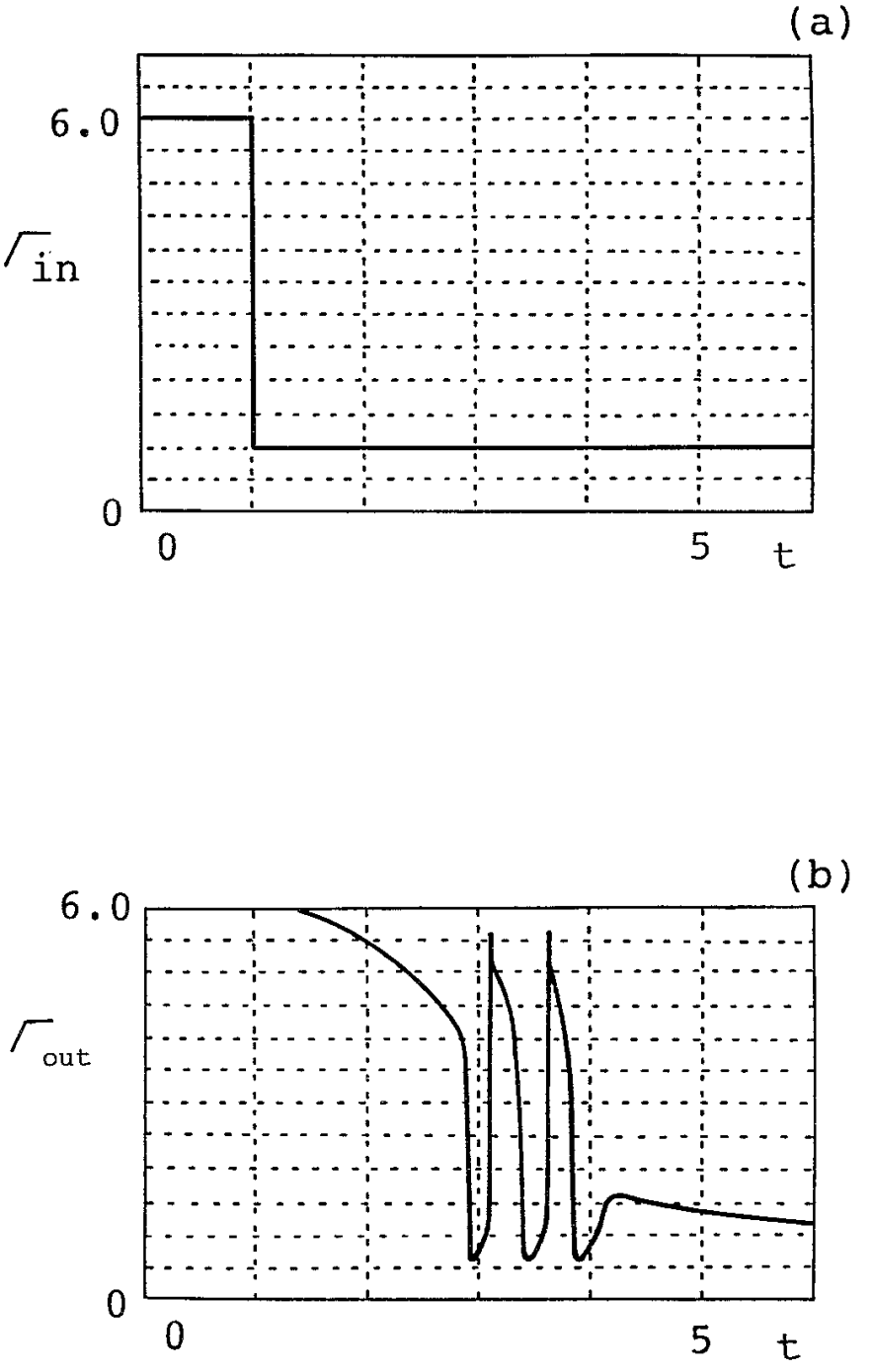

Fig.8

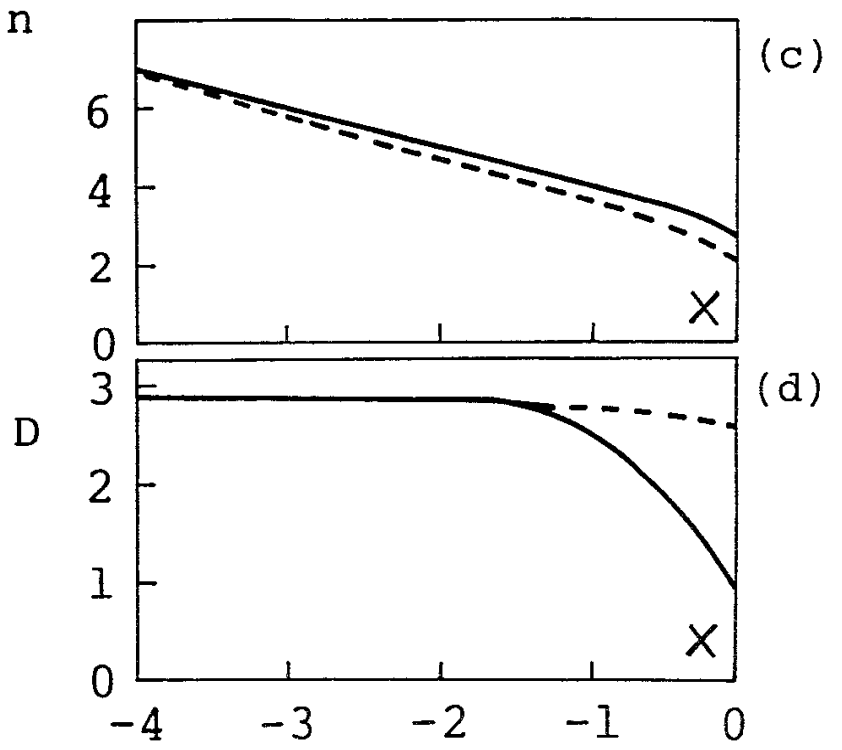

Fig.9

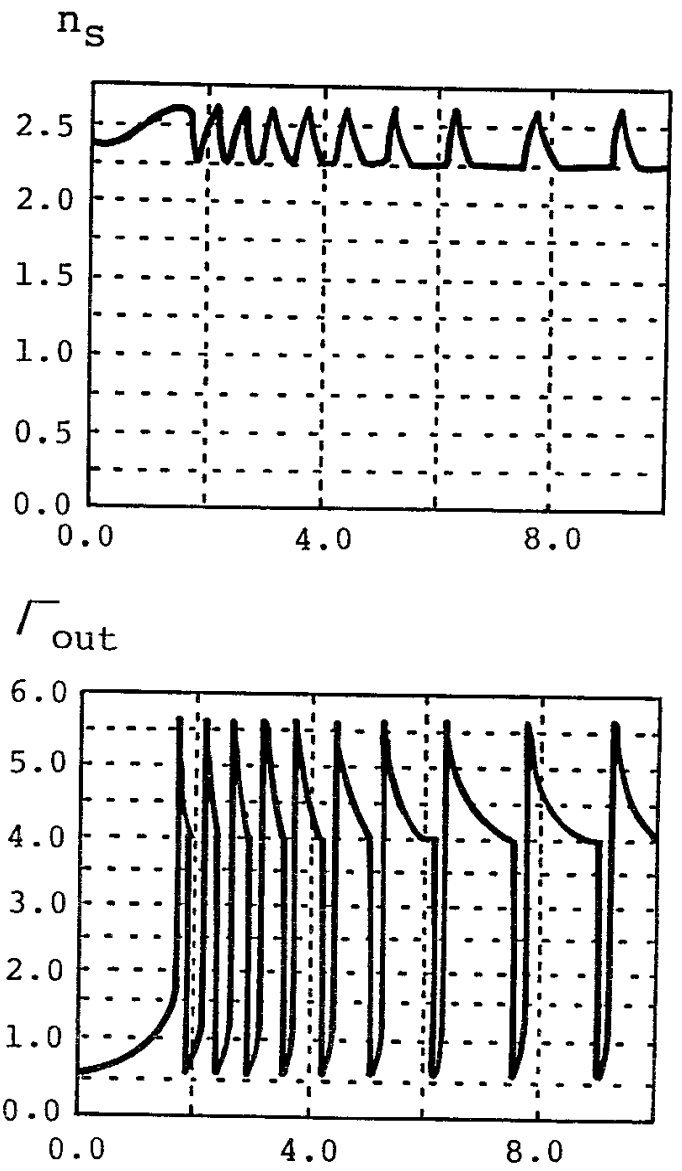

Fig.10

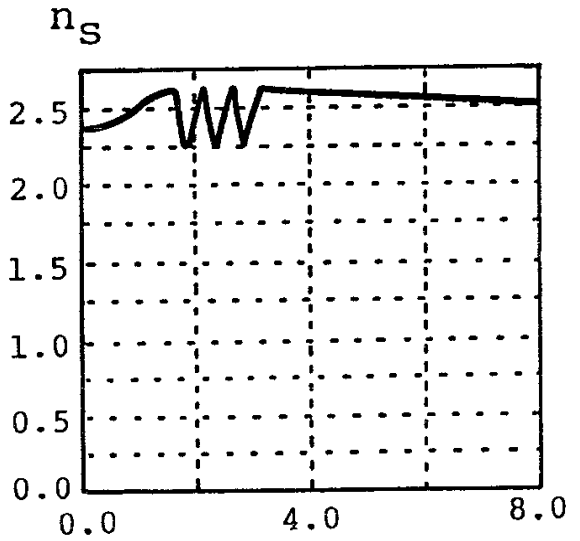

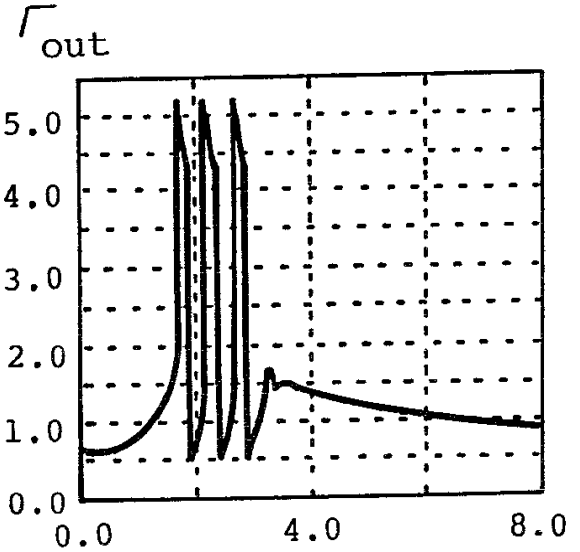

Fig.11

(a)

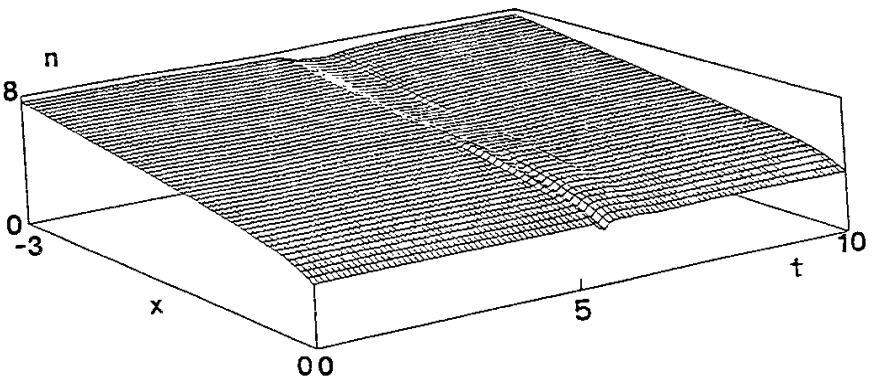

(b)

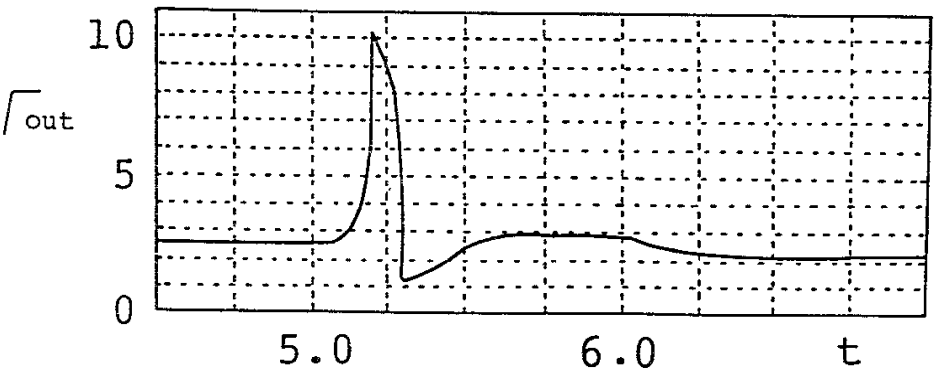

Fig.12

(a)

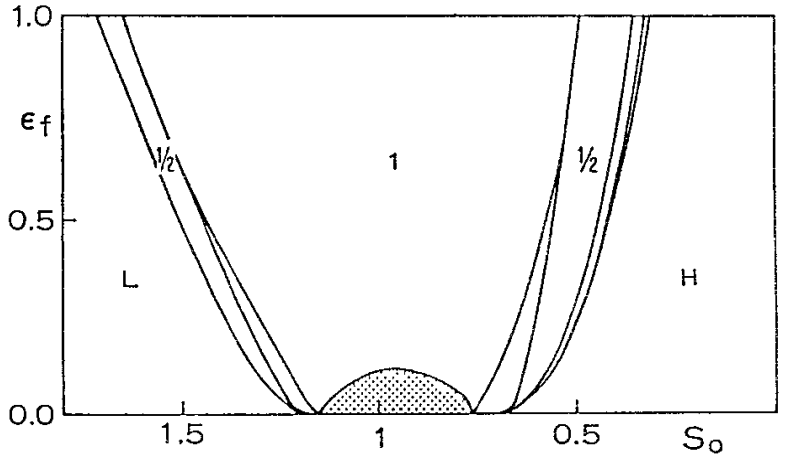
1.0
ϵ_f
0.5
0.0
1/2
1
1/2
L
H
1.5
1
0.5
S_0

(b)

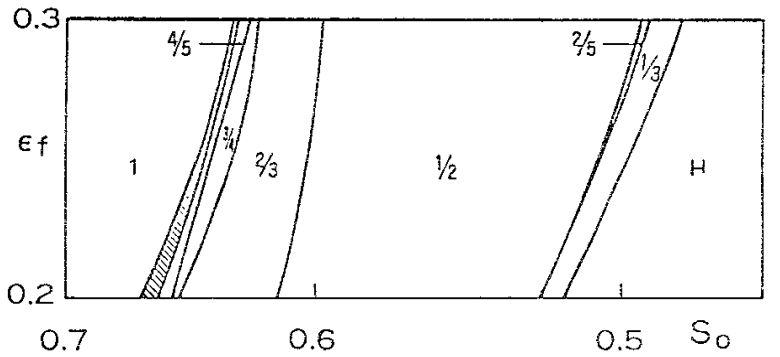
0.3
ϵ_f
0.2
4/5
3/4
2/3
1
1/2
2/5
1/3
H
0.7
0.6
0.5
S_0

Recent Issues of NIFS Series

NIFS-177 N. Ohyabu, K. Yamazaki, I. Katanuma, H. Ji, T. Watanabe, K. Watanabe, H. Akao, K. Akaishi, T. Ono, H. Kaneko, T. Kawamura, Y. Kubota, N. Noda, A. Sagara, O. Motojima, M. Fujiwara and A. Iiyoshi, *Design Study of LHD Helical Divertor and High Temperature Divertor Plasma Operation* ; Sep. 1992

NIFS-178 H. Sanuki, K. Itoh and S.-I. Itoh, *Selfconsistent Analysis of Radial Electric Field and Fast Ion Losses in CHS Torsatron / Heliotron* ; Sep. 1992

NIFS-179 K. Toi, S. Morita, K. Kawahata, K. Ida, T. Watari, R. Kumazawa, A. Ando, Y. Oka, K. Ohkubo, Y. Hamada, K. Adati, R. Akiyama, S. Hidekuma, S. Hirokura, O. Kaneko, T. Kawamoto, Y. Kawasumi, M. Kojima, T. Kuroda, K. Masai, K. Narihara, Y. Ogawa, S. Okajima, M. Sakamoto, M. Sasao, K. Sato, K. N. Sato, T. Seki, F. Shimpo, S. Tanahashi, Y. Taniguchi, T. Tsuzuki, *New Features of L-H Transition in Limiter H-Modes of JIPP T-IIU* ; Sep. 1992

NIFS-180 H. Momota, Y. Tomita, A. Ishida, Y. Kohzaki, M. Ohnishi, S. Ohi, Y. Nakao and M. Nishikawa, *D-^{3}He Fueled FRC Reactor "Artemis-L"* ; Sep. 1992

NIFS-181 T. Watari, R. Kumazawa, T. Seki, Y. Yasaka, A. Ando, Y. Oka,O. Kaneko, K. Adati, R. Akiyama, Y. Hamada, S. Hidekuma, S. Hirokura, K. Ida, K. Kawahata, T. Kawamoto, Y. Kawasumi, S. Kitagawa, M. Kojima, T. Kuroda, K. Masai, S. Morita, K. Narihara, Y. Ogawa, K. Ohkubo, S. Okajima, T. Ozaki, M. Sakamoto, M. Sasao, K. Sato, K. N. Sato, F.Shimpo, H. Takahashi, S. Tanahasi, Y. Taniguchi, K. Toi, T. Tsuzuki and M. Ono, *The New Features of Ion Bernstein Wave Heating in JIPP T-IIU Tokamak* ;Sep, 1992

NIFS-182 K. Itoh, H. Sanuki and S.-I. Itoh, *Effect of Alpha Particles on Radial Electric Field Structure in Torsatron / Heliotron Reactor*; Sep. 1992

NIFS-183 S. Morimoto, M. Sato, H. Yamada, H. Ji, S. Okamura, S. Kubo, O. Motojima, M. Murakami, T. C. Jernigan, T. S. Bigelow, A. C. England, R. S. Isler, J. F. Lyon, C. H. Ma, D. A. Rasmussen, C. R. Schaich, J. B. Wilgen and J. L. Yarber, *Long Pulse Discharges Sustained by Second Harmonic Electron Cyclotron Heating Using a 35GH$_Z$ Gyrotron in the Advanced Toroidal Facility*; Sep. 1992

NIFS-184 S. Okamura, K. Hanatani, K. Nishimura, R. Akiyama, T. Amano, H. Arimoto, M. Fujiwara, M. Hosokawa, K. Ida, H. Idei, H. Iguchi, O. Kaneko, T. Kawamoto, S. Kubo, R. Kumazawa, K. Matsuoka, S. Morita, O. Motojima, T. Mutoh, N. Nakajima, N. Noda, M. Okamoto, T. Ozaki, A. Sagara, S. Sakakibara, H. Sanuki, T. Seki, T. Shoji,

F. Shimbo, C. Takahashi, Y. Takeiri, Y. Takita, K. Toi, K. Tsumori, M. Ueda, T. Watari, H. Yamada and I. Yamada, *Heating Experiments Using Neutral Beams with Variable Injection Angle and ICRF Waves in CHS* ; Sep. 1992

NIFS-185 H. Yamada, S. Morita, K. Ida, S. Okamura, H. Iguchi, S. Sakakibara, K. Nishimura, R. Akiyama, H. Arimoto, M. Fujiwara, K. Hanatani, S. P. Hirshman, K. Ichiguchi, H. Idei, O. Kaneko, T. Kawamoto, S. Kubo, D. K. Lee, K. Matsuoka, O, Motojima, T. Ozaki, V. D. Pustovitov, A. Sagara, H. Sanuki, T. Shoji, C. Takahashi, Y. Takeiri, Y. Takita, S. Tanahashi, J. Todoroki, K. Toi, K. Tsumori, M. Ueda and I. Yamada, *MHD and Confinement Characteristics in the High-ß Regime on the CHS Low-Aspect-Ratio Heliotron / Torsatron* ; Sep. 1992

NIFS-186 S. Morita, H. Yamada, H. Iguchi, K. Adati, R. Akiyama, H. Arimoto, M. Fujiwara, Y. Hamada, K. Ida, H. Idei, O. Kaneko, K. Kawahata, T. Kawamoto, S. Kubo, R. Kumazawa, K. Matsuoka, T. Morisaki, K. Nishimura, S. Okamura, T. Ozaki, T. Seki, M. Sakurai, S, Sakakibara, A. Sagara, C. Takahashi, Y. Takeiri, H. Takenaga, Y. Takita, K. Toi, K. Tsumori, K. Uchino, M. Ueda, T. Watari, I. Yamada, *A Role of Neutral Hydrogen in CHS Plasmas with Reheat and Collapse and Comparison with JIPP T-IIU Tokamak Plasmas* ; Sep. 1992

NIFS-187 K. Ioth, S.-I. Itoh, A. Fukuyama, M. Yagi and M. Azumi, *Model of the L-Mode Confinement in Tokamaks* ; Sep. 1992

NIFS-188 K. Itoh, A. Fukuyama and S.-I. Itoh, *Beta-Limiting Phenomena in High-Aspect-Ratio Toroidal Helical Plasmas*; Oct. 1992

NIFS-189 K. Itoh, S. -I. Itoh and A. Fukuyama, *Cross Field Ion Motion at Sawtooth Crash* ; Oct. 1992

NIFS-190 N. Noda, Y. Kubota, A. Sagara, N. Ohyabu, K. Akaishi, H. Ji, O. Motojima, M. Hashiba, I. Fujita, T. Hino, T. Yamashina, T. Matsuda, T. Sogabe, T. Matsumoto, K. Kuroda, S. Yamazaki, H. Ise, J. Adachi and T. Suzuki, *Design Study on Divertor Plates of Large Helical Device (LHD)* ; Oct. 1992

NIFS-191 Y. Kondoh, Y. Hosaka and K. Ishii, *Kernel Optimum Nearly-Analytical Discretization (KOND) Algorithm Applied to Parabolic and Hyperbolic Equations* : Oct. 1992

NIFS-192 K. Itoh, M. Yagi, S.-I. Itoh, A. Fukuyama and M. Azumi, *L-Mode Confinement Model Based on Transport-MHD Theory in Tokamaks* ; Oct. 1992

NIFS-193 T. Watari, *Review of Japanese Results on Heating and Current*

Drive ; Oct. 1992

NIFS-194 Y. Kondoh, *Eigenfunction for Dissipative Dynamics Operator and Attractor of Dissipative Structure* ; Oct. 1992

NIFS-195 T. Watanabe, H. Oya, K. Watanabe and T. Sato, *Comprehensive Simulation Study on Local and Global Development of Auroral Arcs and Field-Aligned Potentials* ; Oct. 1992

NIFS-196 T. Mori, K. Akaishi, Y. Kubota, O. Motojima, M. Mushiaki, Y. Funato and Y. Hanaoka, *Pumping Experiment of Water on B and LaB_6 Films with Electron Beam Evaporator* ; Oct., 1992

NIFS-197 T. Kato and K. Masai, *X-ray Spectra from Hinotori Satellite and Suprathermal Electrons* ; Oct. 1992

NIFS-198 K. Toi, S. Okamura, H. Iguchi, H. Yamada, S. Morita, S. Sakakibara, K. Ida, K. Nishimura, K. Matsuoka, R. Akiyama, H. Arimoto, M. Fujiwara, M. Hosokawa, H. Idei, O. Kaneko, S. Kubo, A. Sagara, C. Takahashi, Y. Takeiri, Y. Takita, K. Tsumori, I. Yamada and H. Zushi, *Formation of H-mode Like Transport Barrier in the CHS Heliotron / Torsatron* ; Oct. 1992

NIFS-199 M. Tanaka, *A Kinetic Simulation of Low-Frequency Electromagnetic Phenomena in Inhomogeneous Plasmas of Three-Dimensions* ; Nov. 1992

NIFS-200 K. Itoh, S.-I. Itoh, H. Sanuki and A. Fukuyama, *Roles of Electric Field on Toroidal Magnetic Confinement*, Nov. 1992

NIFS-201 G. Gnudi and T. Hatori, *Hamiltonian for the Toroidal Helical Magnetic Field Lines in the Vacuum*; Nov. 1992

NIFS-202 K. Itoh, S.-I. Itoh and A. Fukuyama, *Physics of Transport Phenomena in Magnetic Confinement Plasmas*; Dec. 1992

NIFS-203 Y. Hamada, Y. Kawasumi, H. Iguchi, A. Fujisawa, Y. Abe and M. Takahashi, *Mesh Effect in a Parallel Plate Analyzer*; Dec. 1992

NIFS-204 T. Okada and H. Tazawa, *Two-Stream Instability for a Light Ion Beam -Plasma System with External Magnetic Field;* Dec. 1992

NIFS-205 M. Osakabe, S. Itoh, Y. Gotoh, M. Sasao and J. Fujita, *A Compact Neutron Counter Telescope with Thick Radiator (Cotetra) for Fusion Experiment*; Jan. 1993

NIFS-206 T. Yabe and F. Xiao, *Tracking Sharp Interface of Two Fluids by the CIP (Cubic-Interpolated Propagation) Scheme,* Jan. 1993

NIFS-207 A. Kageyama, K. Watanabe and T. Sato, *Simulation Study of MHD Dynamo : Convection in a Rotating Spherical Shell*; Feb. 1993

NIFS-208 M. Okamoto and S. Murakami, *Plasma Heating in Toroidal Systems*; Feb. 1993

NIFS-209 K. Masai, *Density Dependence of Line Intensities and Application to Plasma Diagnostics*; Feb. 1993

NIFS-210 K. Ohkubo, M. Hosokawa, S. Kubo, M. Sato, Y. Takita and T. Kuroda, *R&D of Transmission Lines for ECH System* ; Feb. 1993

NIFS-211 A. A. Shishkin, K. Y. Watanabe, K. Yamazaki, O. Motojima, D. L. Grekov, M. S. Smirnova and A. V. Zolotukhin, *Some Features of Particle Orbit Behavior in LHD Configurations*; Mar. 1993

NIFS-212 Y. Kondoh, Y. Hosaka and J.-L. Liang, *Demonstration for Novel Self-organization Theory by Three-Dimensional Magnetohydrodynamic Simulation*; Mar. 1993

NIFS-213 K. Itoh, H. Sanuki and S.-I. Itoh, *Thermal and Electric Oscillation Driven by Orbit Loss in Helical Systems*; Mar. 1993

NIFS-214 T. Yamagishi, *Effect of Continuous Eigenvalue Spectrum on Plasma Transport in Toroidal Systems*; Mar. 1993

NIFS-215 K. Ida, K. Itoh, S.-I.Itoh, Y. Miura, JFT-2M Group and A. Fukuyama, *Thickness of the Layer of Strong Radial Electric Field in JFT-2M H-mode Plasmas*; Apr. 1993

NIFS-216 M. Yagi, K. Itoh, S.-I. Itoh, A. Fukuyama and M. Azumi, *Analysis of Current Diffusive Ballooning Mode*; Apr. 1993

NIFS-217 J. Guasp, K. Yamazaki and O. Motojima, *Particle Orbit Analysis for LHD Helical Axis Configurations* ; Apr. 1993

NIFS-218 T. Yabe, T. Ito and M. Okazaki, *Holography Machine HORN-1 for Computer-aided Retrieve of Virtual Three-dimensional Image* : Apr. 1993

NIFS-219 K. Itoh, S.-I. Iton, A. Fukuyama, M. Yagi and M. Azumi, *Self-sustained Turbulence and L-Mode Confinement in Toroidal Plasmas* ; Apr. 1993

NIFS-220 T. Watari, R. Kumazawa, T. Mutoh, T. Seki, K. Nishimura and F. Shimpo, *Applications of Non-resonant RF Forces to Improvement of Tokamak Reactor Performances Part I: Application of Ponderomotive Force* ; May 1993